Structural and Dielectric Properties of Bismuth Doped Cobalt Nano Ferrites Prepared by Sol-Gel Auto Combustion Method

Krutika L. Routray[1*], Dhrubananda Behera[1]
[1]Department of Physics and Astronomy, National Institute of Technology, Rourkela, India
Email: rkruttika@gmail.com

Abstract

The present study is focused on the preparation of a series of Bismuth doped $CoFe_2O_4$ (CFO) nanoparticles and its structural and dielectric properties. The CFO particles having chemical composition $CoBi_xFe_{2-x}O_4$ (where x = 0.0, 0.1, 0.5) has been synthesized using sol-gel auto combustion method. Phase formation study of the prepared samples is carried out using X -ray diffraction (XRD) technique. It reveals single phase spinel structure having space group Fd3m. The two absorption bands ν_1 and ν_2 are observed in Fourier transform infrared spectroscopy (FTIR) spectra corresponding to the tetrahedral and octahedral sites, which show mark of spinel structure of the samples. Morphological study is carried out using Field Emission Scanning Electron Microscope (FESEM) and Transmission Electron Microscopy (TEM) which revealed that the particle size obtained is around 40 nm to 120 nm. In addition, phase formation has been confirmed from the analysis of Raman spectra. Different types of conduction mechanism of the charge carriers have been analysed with DC resistivity and AC impedance measurement at room temperature. Results demonstrate the presence of dielectric relaxation, which is found to be of non-Debye type.

Keywords
Cobalt ferrite ($CoFe_2O_4$), Solgel- auto combustion, Structural properties, Dielectric study

1. Introduction

Spinel-type ferrites have gained importance in recent years because of its extraordinary structural, magnetic, dielectric and electrical properties. $CoFe_2O_4$, being a spinel-type ceramic oxide with Co^{2+} ions at octahedral sites and Fe^{3+} ions equally occupying both tetrahedral and octahedral sites and is a suitable material for developing new technologies in the areas of strategic importance [1,2]. It is one of the essential nanoferrites with high coercivity, moderate magnetization and very high magneto-crystalline anisotropy [3]. Its high negative magneto-striction and capability to withstand at higher frequencies by minimizing the eddy current losses makes cobalt ferrite a suitable and economical material for developing oxide based magneto-strictive materials [4]. Cobalt Ferrite ($CoFe_2O_4$) is a spinel structured ceramic oxide and well recognised hard magnetic material with high coercivity and moderate magnetisation [5].

The doping composition plays a vital role in influencing the properties of Cobalt ferrite by altering its chemical as well as physical properties. $BiFeO_3$ (Bismuth Ferrite) is perhaps the

only material that exhibits both magnetic and a strong ferroelectric behaviour at room temperature and can alter properties of cobalt ferrite due to its high electrical resistivity with low magnetic and dielectric losses. There is a coexistence of interrelated electric and magnetic dipole structures within a certain temperature range in $BiFeO_3$ with perovskite structure. Therefore, Bi_2O_3 is a potential dopant for enhancing the magnetic and electrical properties of ferrites [6]. It is reported that substituting bismuth in very small amount does not alter the spinal structure of Cobalt ferrite [7]. Bismuth doped Cobalt nanoferrites are used for magnetic recording applications such as audio, videotapes, high density data storage devices and microwave device applications [8]. Among several methods to synthesize nanoferrites, the sol-gel auto combustion method is a simple method which quickens up the synthesis of complex materials and brings crystal homogeneity [9]. Hence, in this study, we report the synthesis, its structural characterisations and dielectric properties of Bismuth doped Cobalt nanoferrites with the chemical composition $CoBixFe_{2-x}O_4$ (where x = 0.0, 0.1, 0.5).

2. Experimental details

2.1 Synthesis

A series of Bismuth substituted cobalt nano ferrites having the chemical formula $CoBi_xFe_{2-x}O_4$ (where x = 0.0, 0.1, 0.5) were prepared by sol-gel auto combustion method. The precursors used were Cobalt Nitrate, Iron Nitrate, Bismuth Nitrate and glycine. The stoichiometric amount of all metal nitrates mentioned above was dissolved in a glass beaker with minimum quantity of double distilled water. Glycine was added to the mixed metal solution with molar ratio of nitrates to glycine is 1:4 and mixed together with the help of magnetic stirrer at about 150^0 C with uniform stirring and evaporated to obtain a highly viscous gel. During this procedure, the solution became viscous and finally formed a very homogenous viscous brown gel. The auto-ignition was completed, yielding the black-coloured ashes similar to that of the structure of a branched tree. The as-prepared powders of all the samples were calcined separately at 600^0 C for three hours to get the final product. Further the prepared compositions were characterized by XRD, FESEM, TEM, RAMAN and FTIR followed by Dielectric studies.

2.2 Characterization techniques

The resultant powder was characterized by qualitative X-ray powder diffraction measurements to check the phase purity of the sample with the help of Rigaku X-ray Diffractometer (using Cu-Kα radiation, λ=1.54 Å) at room temperature. X-ray diffraction peaks may be indexed in the space group Fd3m. No trace of impurity was detected by X-ray diffraction. The XRD data for Rietveld refinements were collected over the range of 2θ = 200 – 800 with a step size of 0.020. Revised Rietveld analysis of the X-ray data was carried out by FULLPROF program. Microscopically investigation has been carried out with Nova Nano SEM/FEI field emission scanning electron microscope (FESEM) and FEI transmission electron microscopy (TEM) to determine the particle size. An STR 500 confocal micro-Raman spectrometer (532 nm DPSS laser) was used for Raman spectroscopy. FTIR spectroscopy was carried using Perkin Elmer, USA/ RX-I FTIR. Impedance measurement has been performed using H20KI LCR meter (IM3570) at the room temperature.

3. Results and discussion

3.1 Structural information

3.1.1 *XRD Analysis*

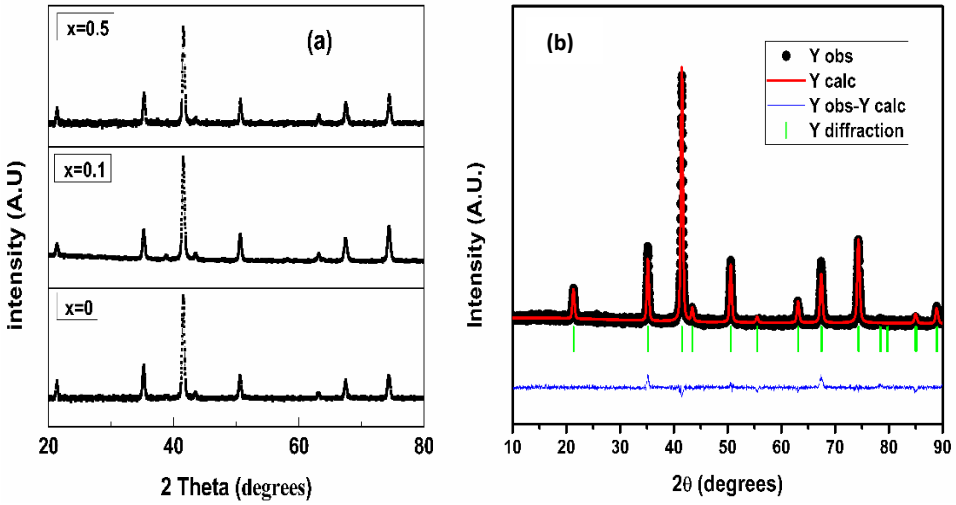

Figure 1. (a) X-ray diffraction patterns of $CoBi_xFe_{2-x}O_4$ (where x = 0.0, 0. 1, 0.5), (b) Reitveld refinement of parent cobalt ferrite ($CoFe_2O_4$).

Figure 1(a) shows X-ray diffraction patterns of $CoBi_xFe_{2-x}O_4$ (where x = 0.0, 0.1, 0.5) nano ferrite particles at room temperature. Generally for a pure cobalt ferrite, the XRD pattern exhibits eight peaks which are located in between $2\theta = 10^0$ to 80^0. The position of the peaks is assigned to cobalt ferrite in accordance with the JCPDS card no 22-1086. The phase shows the pure cubic structure of $CoFe_2O_4$ with as expected inverse spinel lattice [10]. Figure 1 (b) shows the Reitveld refinement which further confirmed the formation of the single phase of parent cobalt ferrite ($CoFe_2O_4$). The inversion parameter ($\boldsymbol{\chi^2}$) calculated from Rietveld refinement is 1.04 mentioned in the equation below:

$$\boldsymbol{\chi^2} = \left[\frac{\boldsymbol{R_{wp}}}{\boldsymbol{R_{exp}}}\right]^2; \qquad (1)$$

where $\boldsymbol{\chi^2}$ is the goodness of Fit of the refinement;
$\boldsymbol{R_{wp}}$ is the weighted pattern of the refinement;
$\boldsymbol{R_{exp}}$ is the calculated pattern of the refinement.

On substitution of Bismuth in a very small amount the spinal structure of ferrite system does not get altered. From the XRD pattern it is identified for x = 0.0, 0.1, 0.5 shows peaks consistent with cubic spinel phase. From the most intense peak of the reflection (311), we have estimated the average particle size of the nanoparticle using Scherrer equation mentioned below:

$$\tau = \frac{K\lambda}{\beta cos\theta}; \qquad (2)$$

where:
τ is the mean size of the ordered (crystalline) domains, which may be smaller or equal to the grain size;
K is a dimensionless shape factor;
λ is the X-ray wavelength;
β is the line broadening at half the maximum intensity (FWHM), after subtracting the instrumental line broadening, in radians;
θ is the Bragg angle (in degrees).

3.1.2 FESEM Study

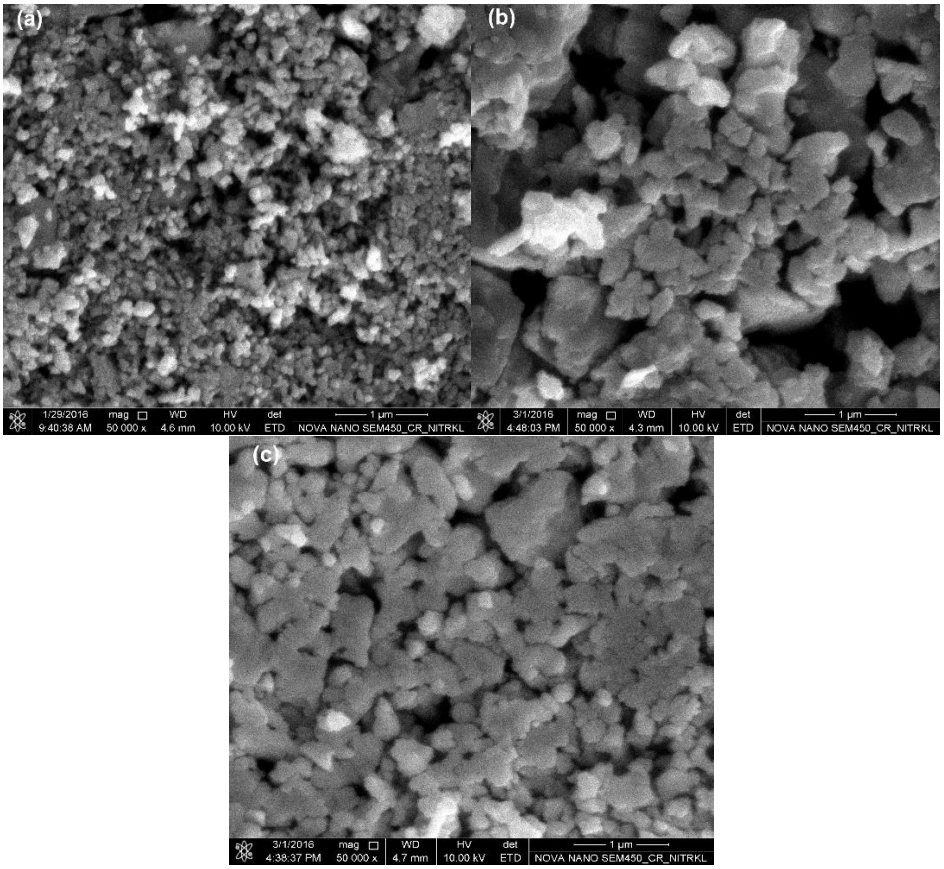

Figure 2. FESEM images of (a) $CoFe_2O_4$ nano ferrite (b) $CoBi_{0.1}Fe_{1.9}O_4$ nano ferrite (c) $CoBi_{0.5}Fe_{1.5}O_4$ nano ferrite.

The Field Emission Scanning Electron Microscope (FESEM) images of the parent and modified cobalt ferrite nano particles ($CoBi_xFe_{2-x}O_4$, x = 0 where x = 0.0, 0.1, 0.5) are shown in Figure 2(a, b, c). It is clear from the FESEM images that the particles have an almost homogeneous distribution and some particles are in agglomerated form. An apparent growth in the particle size is observed which is due to the Bi substitution. Lijun Jia et al. reported a similar behaviour in development of particle size on substitution of Bi in NiCuZn ferrite [11]. The particle size grows controllably from ~ 40 nm in parent to ~ 120 nm in Bi modified cobalt ferrite samples which may be due to the increase in lattice constant which creates

internal strain. With this study it can be observed that the average particle size was in increasing trend with Bi substitution.

3.1.3 TEM Analysis

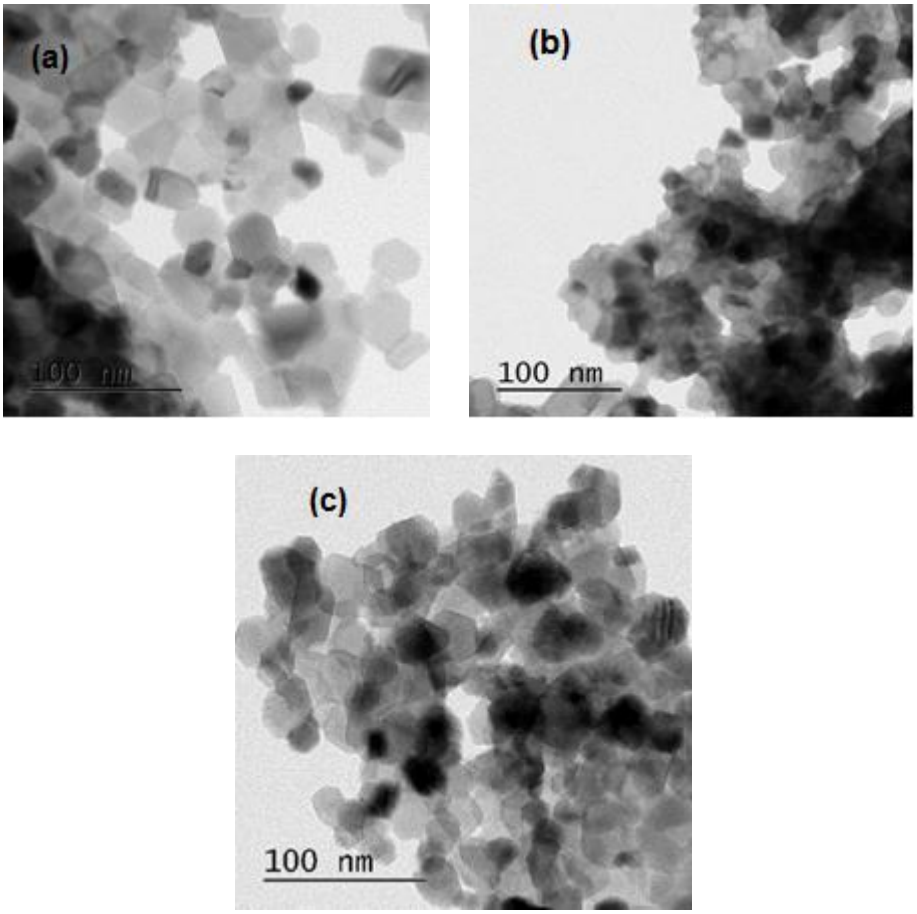

Figure 3. TEM images of (a) $CoFe_2O_4$ nano ferrite (b) $CoBi_{0.1}Fe_{1.9}O_4$ nano ferrite (c) $CoBi_{0.5}Fe_{1.5}O_4$ nano ferrite.

Figure 3 shows the transmission electron microscopy (TEM) image of $CoBi_xFe_{2-x}O_4$, (where x = 0.0, 0.1, 0.5) nanoparticles synthesized at 600^0 C. The average particle size obtained is approximately equal to 40 nm and varies to 90 nm with increase in Bismuth substitution which is in agreement with XRD pattern and FESEM images. The lattice parameter value obtained in all cases is 8.38 Å, which is also in good agreement with the standard value.

3.1.4 RAMAN Study

The samples $CoBi_xFe_{2-x}O_4$, (where x = 0.0, 0.1, 0.5) were further characterised by Raman spectroscopy for further confirmation of phase purity as shown in figure 4. Room temperature Raman spectra of the samples were recorded in the range 0-3000 cm^{-1}. As shown in the figure, strong peaks are observed in range 200 - 800 cm^{-1} and very weak peaks are observed in the range 1000 - 3000 cm^{-1}. The obtained result is in agreement with the XRD results.

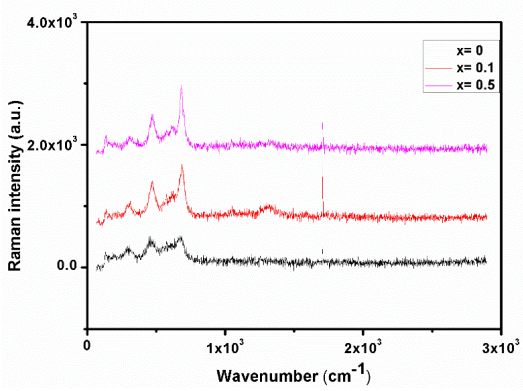

Figure 4. RAMAN spectra of $CoBi_xFe_{2-x}O_4$, (where x = 0.0, 0.1, 0.5).

The resulted peaks in the order of formation are due to the symmetric stretching of oxygen atoms along Fe-O bonds in tetrahedral coordination, symmetric bending of oxygen with respect to the metal ion, asymmetric bending of oxygen, asymmetric bending of Fe (Bi) and O, vibrational modes at octahedral position and translational movement at tetrahedron sites [12].

3.1.5 FTIR Spectra

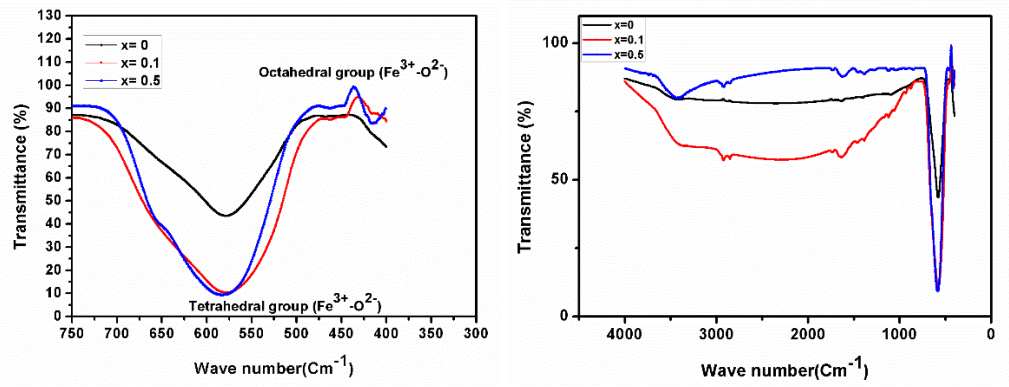

Figure 5. FT-IR spectra of $CoBi_xFe_{2-x}O_4$, (where x = 0.0, 0.1, 0.5).

The FT-IR spectra of $CoBi_xFe_{2-x}O_4$, (where x = 0.0, 0.1, 0.5) nano ferrite particles, synthesised at room temperature is represented in the figure 5. In this present work, we observe three broad features in the frequency range, 3350 - 3500 cm^{-1}, 1600-1647cm^{-1}, 440-600 cm^{-1}.The above broad frequency range corresponds to O-H stretching, H-O-H bending vibration of water molecules and spinal structure with sub-lattices respectively [13]. The presence of frequency bands in this specific range explains the normal mode of vibration of tetrahedral cluster is higher than that of octahedral cluster in the spinel ferrites. The highest one corresponds to the intrinsic stretching vibrations of the metal at the tetrahedral site, whereas the lowest band is assigned to octahedral-metal stretching. This difference between the tetrahedral and octahedral clusters of spinel ferrite is because of the variation in distance between Fe^{3+}- O^{2-} ions in tetrahedral and octahedral sites. The wave band v_1 shows an increase in the values with increase in Bi concentration which may be due to dissimilarity in the cations-oxygen bond length.

3.2 Impedance and modulus of spectroscopy study

The mechanism used to analyse the microstructure-property relationship is the Complex impedance spectroscopy (CIS) which not only helps in distinguishing between intrinsic bulk and extrinsic contributions grain boundary, surface layer, and electrode contact problem but also enables us to separate the real and imaginary component of the electrical parameters so as to get the true picture of the material properties. This technique is based on analysing the ac response of the system to sinusoidal perturbation and subsequent calculation of impedance as a function of frequency of perturbation. The frequency dependence of electrical properties of a material is represented in terms of complex impedance and Z^* electrical modulus (M^*), complex dielectric constant (ε^*) and tangent loss ($tan\delta$) [14]. The following are the complex impedance related parameters:

Complex impedance $Z^* = Z' - jZ'' = R_s - {}^{j}/_{\omega C_s}$; (3)

Complex modulus $M^* = 1/\varepsilon^* = M' + jM'' = j\omega C_0 Z$; (4)

Loss tangent $= \varepsilon''/\varepsilon = M''/M' = -Z'/Z''$; (5)

where Z', M', ε' are the real components of impedance, modulus and permittivity and Z'', M'', ε'' are the imaginary parts of impedance, modulus and permittivity, $j = \sqrt{-1}$ is the Impedance and modulus of spectroscopy study is the imaginary factor and $\omega = 2\pi f$ is the angular frequency. Inverse spinel ferrites namely cobalt ferrite possess good dielectric properties, depending on the size of the particle, distribution of cation and the method of preparation. Dielectric properties (real and imaginary parts of impedance, relative permittivity, dielectric loss tangent) for the prepared series of $CoBi_xFe_{2-x}O_{4,}$ (x = 0.0, 0. 1, 0.5) have been studied in the frequency range 100 Hz- 1 MHz at room temperature.

3.2.1 Impedance study

In order to analyse the electrical properties of spinel type ferrites Impedance analysis is used to determine the contribution of conductivity for both resistive (real part) and reactive (imaginary part) when AC field is applied [15]. Nyquist diagrams also known as Cole-Cole plots or Complex impedance plot gives a complete contribution of microstructure (grains and grains boundary) resistances and helps to differentiate the grain and grain boundary resistances and interfacial resistance of conducting electrodes. Figure 6 (a) and (b) shows the variations of real parts and imaginary parts of complex impedance with applied frequency (100 Hz-1 MHz). From the plots it is observed that up to a definite limiting range (~10 kHz) Z' decreases monotonically with increasing frequency thereafter they merge together and becomes nearly independent of frequency. The higher values of Z' at lower frequencies indicate that the polarization effect in the sample is larger. The values of Z" decreases identically monotonically up to a certain frequency limit (~100 kHz) beyond which they merge together at a very low value of Z" where frequency-independent nature of variation is observed till the highest frequency limit at room temperature for the varying concentration of bismuth doped cobalt nano-ferrite samples.

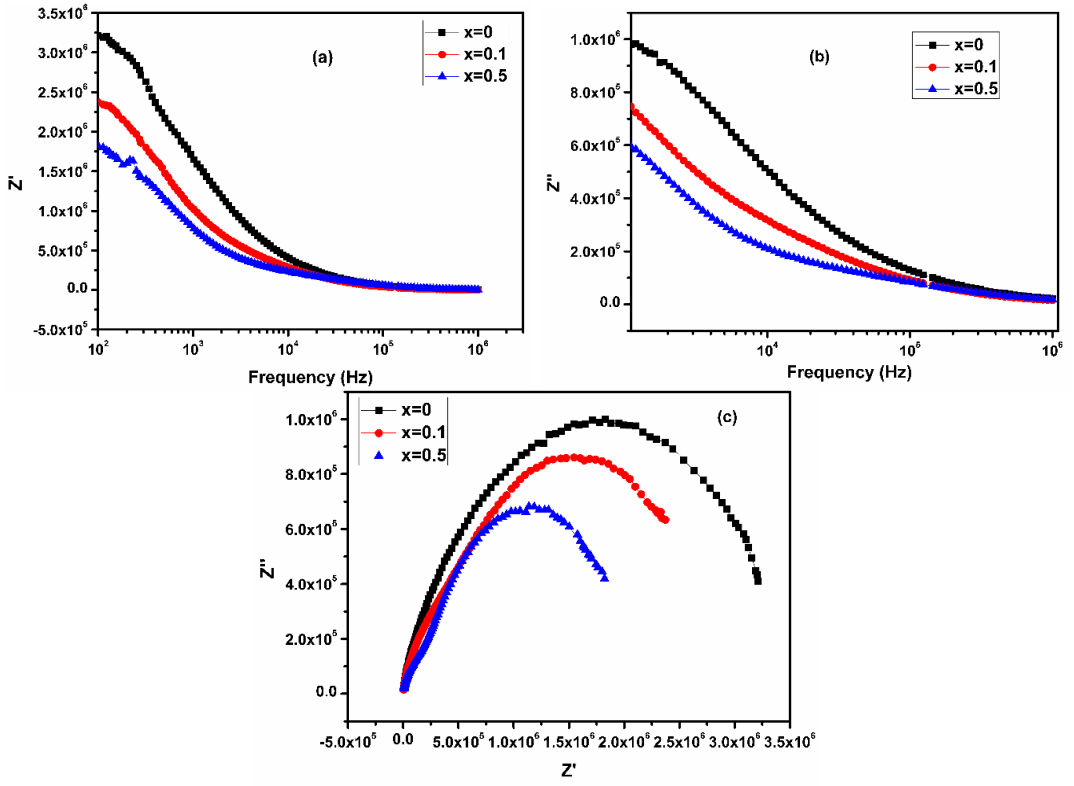

Figure 6. (a) Real part of impedance with applied frequency, (b) imaginary part of impedance with applied frequency (c) the complex impedance plane plots (Cole-Cole) for $CoBi_xFe_{2-x}O_4$, (where x = 0.0, 0.1, 0.5).

This merging of Z' and Z'' at higher frequencies specifies the probable discharge of space charge accumulation at the boundaries of the homogeneous phases in the sample when on application of AC field. It is observed that both the resistance (Z') and reactance (Z'') values decreases with increase in applied AC field concluding that the conduction is stimulated by application of AC field. As observed there is a monotonic decrease in the values of Z' and Z'' with increasing frequencies for all the samples which indicates that relaxation behaviour in the material is dependent on the temperature and no single relaxation time is present. To further examine and differentiate the microstructure such as intrinsic (grain) and extrinsic (interfaces like grain boundary, sample-electrode effect, defects, and relaxation process etc.) Cole-Cole of impedance (Z' vs. Z'') is plotted. Appearance of semicircle in the plot represents a relaxation process, whose radius measures the resistance of the sample and centre lies on the abscissa (Z' - axis) if the conduction is of Debye type. For a non-Debye type conduction process, a depressed semicircle appears in the diagram. For the appearance of three distinct semicircles in the diagram, the one appears at high frequency end is assigned to grain effect, the semicircle at intermediate frequency zone corresponds to grain boundary effect and that of at lower frequency end is ascribed to sample surface conduction effect [16]. We observe only one Cole-Cole semicircle in the plot where the radius of the semicircle decreases with increases in Bismuth concentration indicating the decrease in resistance of the material. All the curves show a tendency to bend towards the abscissa to form semicircles with their centres above the real axis, having comparatively decreased in radii. Though a single relaxation process is observed in the experimented temperature range it is tough to assign that

the change in behaviour is due to intrinsic conduction effect as the resistance of the material is sufficiently low to prevent the arrival of extrinsic interfacial conduction effect.

In order to properly differentiate between the intrinsic and extrinsic consequence on conduction mechanism we illustrate the frequency dependent imaginary part of Modulus (M'') in Figure 7 to verify the relaxation behaviour.

3.2.2 Complex Modulus Analysis

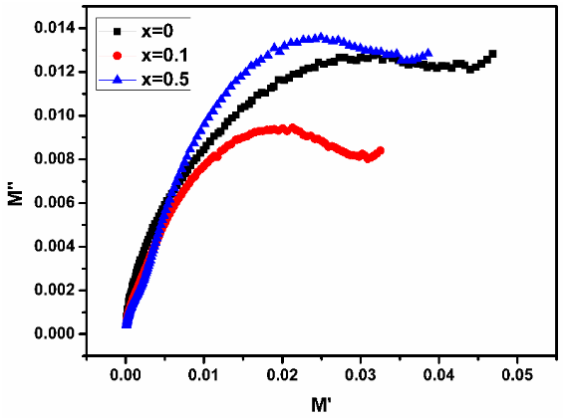

Figure 7. Complex modulus plots for $CoBi_xFe_{2-x}O_4$, (where x = 0.0, 0.1, 0.5) corresponding to the room temperature measurement.

An alternative method to explore the electrical properties of the material as a result of different relaxation time constants and expand any other properties present in the sample (which are unidentifiable or overlapping in CIS technique) complex modulus analysis is used. It is used to determine the dynamical aspects of electrical transport phenomena (carrier/ion, hopping rate, conductivity relaxation time, etc.). Electric modulus as a parameter varies inversely to the capacitance of the material and hence has the ability to suppress the highest capacitive region of sample-electrode surface conduction effect and highlight the least capacitive grain conduction effect [17]. We observed only one peak in Z' vs. Z'' plots but in case of M' vs. M'' plot, two peaks are observed at room temperature for all the compositions taken. Figure 7 shows the complex modulus plots for $CoBi_xFe_{2-x}O_4$, (x = 0.0, 0.1, 0.5) corresponding to the room temperature measurement. From this figure, we observe that the modulus spectrum has a typical pattern characterized by the presence of little asymmetric and depressed semi-circular arcs with its centre not lying on M' axis, thereby indicating non-Debye type of relaxation response in the investigated material system. The behaviour of the modulus spectrum on right-side semicircles represent values corresponding to higher frequencies and left semicircles corresponding to lower frequencies for the variation in concentration of Bismuth. These semicircles indicate that both grain and grain boundary capacitance play vital roles in the conduction mechanism of the material system at the measured temperature. The behaviour of electric modulus spectrum is indicative of the temperature dependent hopping type of mechanism for electric conduction (charge transport) in the investigated material system and non-Debye type dielectric relaxation.

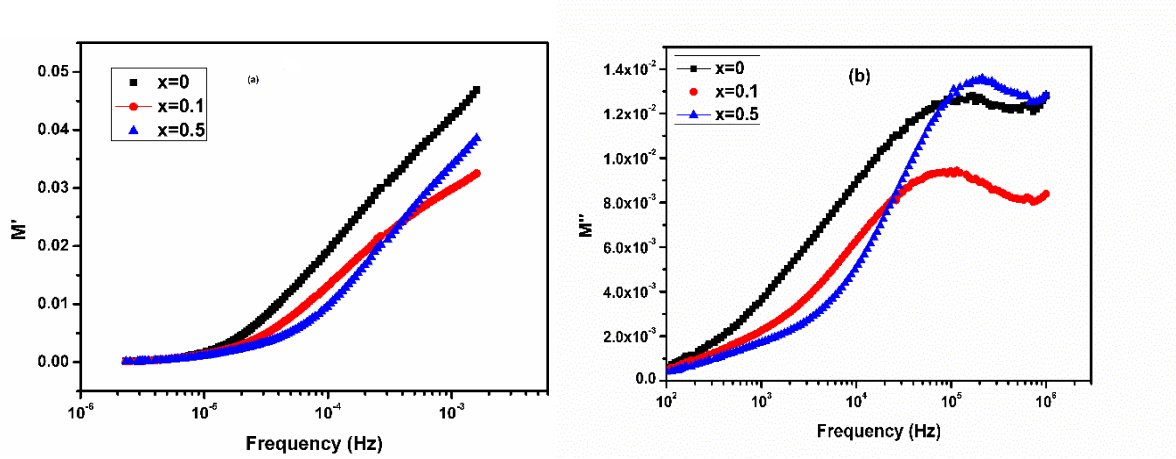

Figure 8. (a) Real part of impedance with applied frequency, (b) imaginary part of impedance with applied frequency of $CoBi_xFe_{2-x}O_4$, (where x = 0.0, 0.1, 0.5).

Figure 8(a) shows the variation of Real part (M') of modulus with frequency at room temperatures of $CoBi_xFe_{2-x}O_4$, (where x = 0.0, 0.1, 0.5). The variation of M' with frequency shows a dispersion tending towards the asymptotic plot of M' at higher frequencies which is due to the relaxation time of the sample. A monotonous dispersion occurs with increasing frequency at room temperature which is because of the short range mobility of charge carriers. Such observed behaviours may be associated with the absence of restoring force that governs the mobility of the charge carriers under the influence of an induced electric field. Figure 8(b) represents the variation of imaginary part of modulus (M") with frequency at room temperatures for variable Bismuth concentration ($CoBi_xFe_{2-x}O_4$, where x = 0.0, 0.1, 0.5). It is observed from the graph that M" indicates the presence of strong peaks and the position of the peaks (M") get shifted to higher frequencies with increase in Bismuth concentration. It is observed that the peaks are asymmetric and broader than the ideal non-Debye curve.

4. Conclusions

In this present work, structural, dielectric, and impedance / modulus conductivity studies on $CoBi_xFe_{2-x}O_4$, (x = 0.0, 0.1, 0.5) in the frequency range 100 Hz-1 MHz in the room temperature is reported. The XRD pattern confirms that sample has a cubic structure at room temperature. Dielectric properties of sample have been carried out in the frequency range 100 Hz - 1 MHz. Impedance spectroscopy concluded the presence of single semicircle arc at all reported temperatures which indicate that there is presence of grain interior (bulk) property in material. The samples showed presence of dielectric relaxation, which is found to be of non-Debye type. As has been observed, the particle size increases with Bi doping, the resistance of the material is decreased. The semicircles in the complex modulus plot indicated that both grain and grain boundary capacitance play a vital role in the conduction mechanism of the material system at the measured temperature.

References

[1] Cheng F, Liao C, Kuang J, Xu Z, Yan C, Chen L, Zhao H and Liu Z 1999 *J. Appl. Phys* **85(5)** 2782-6.
[2] Ryu J, Priya S, Uchino K and Kim HE 2002 *J. Electroceram* **8(2)** 107-19.

[3]Maaz K, Karim S, Mashiatullah A, Liu J, Hou MD, Sun YM, Duan JL, Yao HJ, Mo D and Chen YF 2009 *Physica B: Condensed Matter* **404(21)** 3947-51.
[4] Bhame SD and Joy PA 2007 *J. Phys. D: Appl. Phys* **40(11)** 3263.
[5] Chen W, Zhu W, Tan OK and Chen XF 2010 *J. Appl. Phys* **108(3)** 034101.
[6] Ghosh S, Dasgupta S, Sen A and Sekhar Maiti H 2005 *J. Am. Ceram. Soc* **88(5)** 1349-52.
[7] Kumar NS and Kumar KV 2015 WJNSE **5(04)** 140.
[8] Gupta N, Dimri MC, Kashyap SC and Dube DC 2005 *Ceram. Int* **31(1)** 171-6.
[9] Jo W, Dittmer R, Acosta M, Zang J, Groh C, Sapper E, Wang K and Rödel J 2012 J. *Electroceram* 2012 **29(1)** 71-93.
[10] JCPDS data base 22-1086.
[11] Jia L, Zhang H, Wu X, Li T, Su H. and Liu B 2012 *J. App. Phys* **111(7)** 07A326.
[12] Romþeviü M, Milutinoviü A and Romþeviü NŽ 2012 *Sci. sinter* **44** 331-9.
[13] Faheim AS, Abd El Fattah MK, Abdul Rahman AH and Badawi A 2014 *J. Nanomater. Mol. Nanotechnol* **5** 4-10.doi: http://dx. doi. org/10.4172/2324-8777.100015
[14] Pattanayak S, Priyadarshan A, Subudhi R, Nayak RK and Padhee R 2013 *J. Adv. Ceram* **2(3)** 235-41.
[15] Farea AM, Kumar S, Batoo KM, Yousef A and Lee CG 2008 *J. Alloys Compd* **464(1)** 361-9.
[16] Irvine JT, Sinclair DC and West AR 1990 *Adv. Mater* **2(3)** 132-8.
[17] Sinclair DC and West AR 1989 *J. Appl. Phys* **66(8)** 3850-6.